Nonequilibrium steady states in a vibrated-rod monolayer: tetratic, nematic, and smectic correlations

Nonequilibrium steady states in a vibrated-rod monolayer: tetratic, nematic, and smectic correlations

Vijay Narayan[1]**, Narayanan Menon**[1,2] **and Sriram Ramaswamy**[1]

[1] Centre for Condensed Matter Theory, Department of Physics, Indian Institute of Science, Bangalore, India
[2] Department of Physics, University of Massachusetts, Amherst, USA
E-mail: vj@physics.iisc.ernet.in

Abstract. We study experimentally the nonequilibrium phase behaviour of a horizontal monolayer of macroscopic rods. The motion of the rods in two dimensions is driven by vibrations in the vertical direction. In addition to varying packing fraction and aspect ratio as in most studies on hard-particle systems, we take advantage of our ability to vary the precise shape of these macroscopic particles to investigate the effect of shape on their nonequilibrium steady states. We find that the shape plays an important role in determining the nature of the orientational ordering at high packing fraction. Cylindrical particles show substantial tetratic correlations over a range of aspect ratios where spherocylinders have previously been shown to undergo transitions between isotropic and nematic phases. Particles that are thinner at the ends (rolling pins or bails) show nematic ordering over the same range of aspect ratios, with a well established nematic phase at large aspect ratio and a defect-ridden nematic state with large-scale swirling motion at small aspect ratios. Finally, long-grain, basmati rice, whose geometry is intermediate between the two shapes above, shows phases with strong indications of smectic order.

Contents

1. Introduction

Our experiments study the orientational ordering of horizontal, quasi-two-dimensional assemblies of millimetre-sized, elongated particles driven into motion by external vibration in the vertical direction. Since the particles we study are rod-like and do not deform appreciably, the natural point of comparison is the phase behaviour of thermal equilibrium hard-rod systems in two dimensions. The experiments address some basic questions on how systems in driven, nonequilibrium steady states differ in their phase behaviour and dynamics from similar systems at thermal equilibrium: can the nonequilibrium phase diagram be rationalized by a comparison to hard-rod Monte Carlo simulations [1] alone or must we invoke new physics? In thermal equilibrium, the ordering of hard-rod liquid crystals is determined solely by geometrical considerations of packing, which should apply equally in the molecular and macroscopic realms. On the other hand, thermal fluctuations are of no importance in the systems we report in this article, and all exploration of phase space is made possible only by means of external driving forces.

    The nonthermal nature of the system has several implications: well established extremal principles involving free energy and entropy cannot be invoked, the sources of fluctuation and dissipation are distinct, and nonequilibrium fluctuations may either help or hinder certain kinds of order. 'Moving XY models' of flocking [2, 3], for instance, have been shown to display true long-range order in two dimensions, unlike their equilibrium counterparts. Nonequilibrium steady states with strictly nematic order [4] are predicted

to have anomalously large density fluctuations, and velocity autocorrelations that decay much more slowly than in corresponding thermal systems. There are also a number of papers [5]–[8] on the dynamics of orientable systems that are motivated by the biologically important motor-microtubule system. These systems support a variety of nonequilibrium structures, in particular rotating vortices, which have no equilibrium analogue. While the particles in these systems are polar in nature and therefore not directly comparable to our particles, they do show the possibilities of qualitatively new phases and defect behaviours in systems of driven orientable particles [9, 10].

In the context of nonthermal systems like granular media, Edwards and co-workers have taken an entirely different theoretical approach: they propose a statistical mechanics for granular systems by constructing an ensemble that includes with equal probability all mechanically stable realizations of a system. The phase behaviour of a system of anisotropic grains has been considered [11] within this framework. The theory predicts, remarkably, that elongated particles do not undergo an isotropic-to-nematic transition as a function of density.

There have also been some recent experiments and simulations on the packing of anisotropic granular particles under gravity. Monte Carlo [12] simulations of ellipses falling in two dimensions found that they tend to orient with their long axes perpendicular to gravity. Quasi-2D experiments and simulations [13] on cylinders showed similar results, with nematic ordering extending over two particle lengths. Villarruel *et al* [14] studied the compaction of rods in three dimensions: rods were poured into a cylindrical container and compacted by 'tapping' i.e. applying isolated vertical jolts. While quantitative measures of orientational order were not presented, it was observed that repeated tapping caused the rods to orient vertically, first at the walls and then in bulk, into smectic-like layers. Blair *et al* [15] have studied vibrated systems of rods, contained in circular and annular geometries. At high packing fractions, the rods separated into regions where they are stacked horizontally, and regions in which rods came out of the horizontal plane and are only slightly tipped from the vertical; in the latter regions, vortices formed, rotating in a direction governed by the tilt of the rods. A phenomenological explanation for the formation and motions of the vortices was proposed in [16]. Although we do report on nonequilibrium dynamical effects such as these, our major preoccupation here is with static orientational ordering. Also, the role of gravity in our experiments is to be distinguished from those reported in [12]–[14]: while gravity is very important in the kinematics of the particle motion it does not play the role of an ordering field as in [12]–[14]. The ordering in our system arises purely from interparticle interactions. Measurements of the isotropic–nematic transition in a quasi-2D system of vibrated rods have also been reported by [17]. The focus in that paper is on understanding the long-wavelength distortions of the director in terms of competition between wall alignment and bulk elasticity. Experiments very similar in intent to ours have been performed by Fraden and co-workers [18][3].

While there are no firmly founded theoretical predictions to guide the effort of charting out a nonequilibrium phase diagram for elongated particles, simulations of hard rods in equilibrium provide a valuable point of reference. Frenkel and others [1, 19] have performed Monte Carlo simulations in two dimensions, on spherocylinders of length L and diameter

---

[3] These experiments were done with cylindrical particles in a two-dimensional cell in a horizontal plane. The agitation was provided by repeated tapping in the plane of the cell, rather than by continuous vibration transverse to the cell as in our experiment.

D. They find that nematic phases do not form for particle aspect ratio $\mathcal{A} \equiv L/D < 7$. Instead, they identify an isotropic phase at low number densities and a layered solid at high densities. For particles with $\mathcal{A} > 7$ a nematic phase intervenes at intermediate area fractions. In a grand canonical Monte Carlo study in two dimensions, Khandkar and Barma [20] confirm the quasi-long-range nature of nematic ordering in the 'needle' (i.e., $D = 0$) limit, and demonstrate that imposed gradients in the chemical potential suppress director fluctuations. A recent Monte Carlo simulation [21] studies the ordering of rectangles with $\mathcal{A} = 2$ and finds a transition from isotropic to tetratic order. In an earlier work Veerman *et al* [22] report the occurrence of a cubatic phase in a system of truncated spheres, and more recently Borukhov *et al* [23] find cubatics in linker-filament models for the cytoskeleton. While we are able to make a detailed comparison to these equilibrium simulations, due to the macroscopic nature of the particles we are also able to explore a new axis in the study of hard-rod systems: we can make essentially arbitrary variations in the shape of the particles by selectively etching cylindrical rods. We find a surprising dependence on the precise shape of the particle—objects with similar aspect ratios but dissimilar shapes order differently. It is not possible to determine on the basis of our work alone whether this shape-sensitivity is a nonequilibrium effect; however, we hope to stimulate more detailed investigations of these effects in hard-particle simulations.

Following this introductory section is an experimental section 2, in which we describe the particles used in our study, the geometry of the cell, and the driving mechanism. The system is visualized by real-space images; the acquisition and analysis of the images is also outlined. A detailed description of our results is given in section 3, but we summarize these briefly here: strictly cylindrical particles show substantial tetratic (that is, fourfold orientational) correlations at both small ($\mathcal{A} = 4.9$) and large ($\mathcal{A} = 12.6$) aspect ratio. The length scale of the correlations increases as the number density is increased; however, we do not see long-range order (LRO) over the range of area fractions and vibration amplitudes we explore. Particles that are thinner at their tips ('rolling pins' or 'bails', see figure 1) show nematic ordering at high area fractions in the same range of aspect ratios. For shorter particles ($\mathcal{A} = 5.2$) we obtain a defect-ridden nematic state with large-scale swirling motion at the number densities we study in our experiment. For $\mathcal{A} = 10.4$, we find at high densities a phase with at least quasi-long-range nematic order (QLRO), that is, power-law decay of nematic correlations. We can induce transitions out of this nematic phase either by lowering number density or by increasing the intensity of the driving. Finally, long-grain, basmati rice, with an aspect ratio of $\mathcal{A} \approx 4$, shows phases with strong indications of smectic order. We comment on this below in section 3.3. We also find intriguing dynamical phenomena, with clear signatures of nonequilibrium behaviour, as discussed at the end of section 3.

2. Experimental set-up and procedure

Our experiments involve vertically shaking a horizontal layer of rod-like particles. The rods were confined to a single layer between an aluminium substrate and a lid that fitted over the particles, leaving them only a little vertical room to move in. In this section we describe the particles, the geometry of the experimental cell, the driving mechanism, and, finally, the methods of image acquisition and analysis.
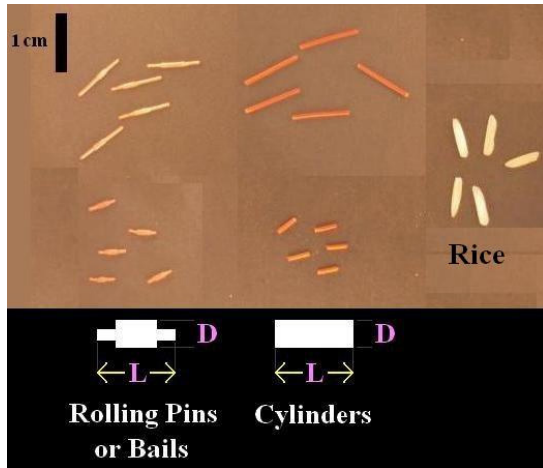
Figure 1. The five kinds of particles we used in our experiments. White silhouettes are schematic outlines of the 2D projections of the particles. We call particles with a strictly rectangular profile 'cylinders' and the others 'rolling pins' or 'bails'. We define the aspect ratio as $\mathcal{A} \equiv L/D$ where the diameter D is measured at the largest cylindrical cross-section. Far right: basmati rice grains. For details of size and polydispersity of the particles see table 1.

Table 1. Details of the various particles we used in our experiments.

	Aspect ratio	Length (mm)
Rice	4.0 ± 1.07	7.1 ± 0.44
Short cylinders	4.9 ± 0.42	3.7 ± 0.11
Short rolling pins	5.2 ± 0.59	4.6 ± 0.16
Long cylinders	12.6 ± 0.66	9.9 ± 0.12
Long rolling pins	10.4 ± 1.45	9.2 ± 0.39

2.1. Particle dimensions

We used five different kinds of particles in the experiment. Figure 1 shows images of a few of each. The particles labelled 'cylinders' are cut from a length of enamelled copper wire. The process of cutting introduces only a small degree of polydispersity ($<5\%$) in the length of the cylinders. The particles labelled 'rolling pins' (or 'bails'[4]) are produced by etching the tips of the cylinders in ferric chloride solution. Since there are variations in the local etch rate, and in the exact length of rod that is exposed to the etchant, the degree of polydispersity in the bails is somewhat greater. The rice was used as purchased. Table 1 summarizes the dimensions of the particles used in the experiment.

2.2. Geometry of the cell

The particles were confined in a shallow circular geometry with a 13 cm diameter, as shown in figure 2. Whenever necessary, it was possible to further confine the particles to

---

[4] The particles we call 'bails' resemble a piece of cricket equipment of the same name.
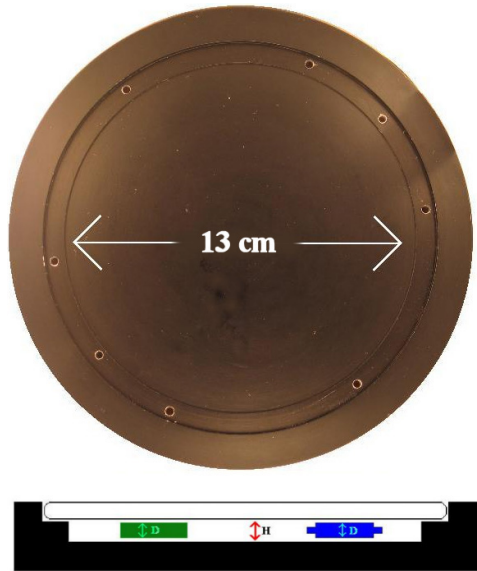
Figure 2. Top and side view of base of circular sample cell. The height of the sample volume, $H = 1.0$ mm, and the diameter of the particles, $D = 0.8$ mm.

a square region inscribed within the diameter of the cell. The base of the cell is made of aluminium, anodized black to enhance optical contrast with the particles. The top of the cylinder is made of Perspex, and is placed so as to leave a vertical space $H = 1$ mm above the base. Since the particles have a diameter $D \simeq 0.8$ mm, this gives them about 25% of their thickness to explore in the vertical direction. Thus particles cannot pass over one another by moving out of plane. The vertical degree of motion allows the planar projection of the particles to overlap a little when they are being shaken; the horizontal component of the distance of closest possible approach of two particles is slightly less than D. Thus, the vertical clearance $H-D$ can be seen as a parameter that tunes the particle interaction potential from hard-core repulsion ($H - D = 0$), when the motion is strictly two dimensional, to slightly softened repulsion for $H > D$. The shaking amplitude a_0 can then be seen as playing the role of temperature.

Another important feature of the cell is the boundary condition presented to the particles at the edge of the system. When the boundary is smooth, particles tend to lie parallel to the boundary. This occurs both when the boundary is a square or a circle since in the latter case the radius of curvature is much larger than the particle length. The parallel alignment is a consequence of dynamical stability: when a rod aligned with the wall collides with it at one end and rotates out of alignment, then the next wall collision will be with the other end of the rod, which will tend to restore the alignment. Such natural alignment parallel to the walls makes it difficult to obtain single-domain orientation in the bulk of the sample, because the alignment favoured by, say, the north–south walls is perpendicular to that imposed by the east–west walls. The formation of a single domain can be promoted by gluing a layer of rods normal to one pair of walls which face each other. The boundary condition at all walls will then favour alignment in the same direction in the horizontal plane. We found this procedure to be effective only for the bails, and not for the cylinders.

2.3. Excitation mechanism

The cells were filled with particles to a known area fraction and then mounted on a permanent magnet shaker (LDS 406). For most of the experiments described here, the cell was shaken at a frequency $f = 200$ Hz and an amplitude a_0 resulting in a fixed peak acceleration, as measured by an accelerometer (PCB Piezotronics 352B02), of $\Gamma \equiv (2\pi f)^2 a_0 = 6g$ where g is the acceleration due to gravity. The corresponding amplitude typically used was $a_0 = 0.037$ mm $= 0.046D$, smaller than the clearance of $H - D = 0.2D$ between the top of the particle and the lid. However, the characteristic velocity of the plate $(2\pi f a_0)$ is sufficient to launch particles to a height of ~ 0.1 mm. We also performed experiments in which we varied the acceleration between $5g$ and $8g$ to observe the effect it had on the degree of ordering.

2.4. Image acquisition and analysis

Dynamical features of the steady states were imaged with a high-speed video camera; however, for the majority of the results reported in this article, our primary interest was the instantaneous configurations of the particles. These were imaged using a consumer digital camera (Canon PowerShot G5) placed above the cell. Images were taken at a resolution of 2592×1944 pixels, at time intervals of approximately 15 s. This interval was long enough for significant rearrangements of the particles to have taken place, and hence for each image to be a statistically independent sampling of the steady state arrangement of the particles. In the rest of this article, we will discuss data extracted from images that were taken while the sample was being continuously agitated by the shaker. Images taken by halting the drive (as done in [18]) showed qualitatively similar behaviour but with noticeably greater disorder in the particle arrangement.

The images were analysed within the ImageJ [25] analysis software. The images were subjected to a bandpass filter to remove pixel noise and long-wavelength variations in illumination, and then thresholded before identifying the centre of mass and orientation of each particle. In the long cylinders and bails, the error in locating the centre of mass of the particle was $0.1\,L$ in the axial direction and $0.1\,D$ in the radial direction. We were able to reduce this error to $0.02\,D$ and $0.02\,L$, respectively, for the short cylinders. The error in assigning the angles was less than $2.5°$. Figure 3 has bars indicating the centres of mass and orientation of the particles superimposed on the image. Typically, 97% of the particles were successfully identified, the remaining particles being difficult to resolve as independent objects because of the high packing density, and the consequent lack of intensity gradient between particles. The other objects identified are mainly particle pairs; we are able to determine the position and orientation of some, but not all, by using information on the minor and major axes of the composite object. However, due to the relatively small number of such instances, they did not affect the results we report here.

3. Results

This section is organized in the following manner: the first half will be devoted to results obtained using the cylinders and the latter half to those with the rolling pins. While the rice grains show excellent layering we are not able to pursue quantitatively the nature
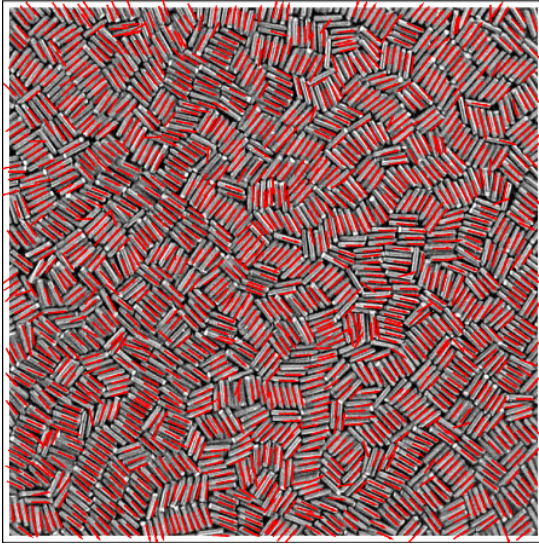
Figure 3. Particles identified by the image analysis routine: each identified particle was assigned a centre-of-mass coordinate and an orientation, indicated by the location and orientation of the bars in the image. Even at these high area fractions, typically 97% of particles were identified.
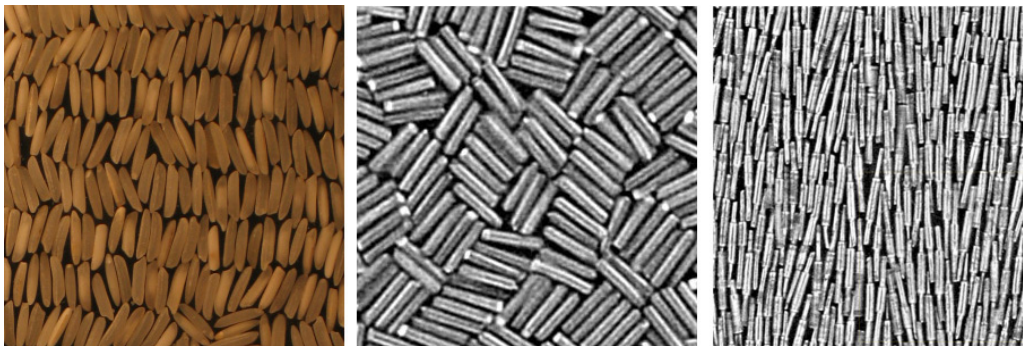

Figure 4. Real space images of steady states observed: striped, smectic-like state with the basmati grains (left), state formed by aspect ratio $\mathcal{A} = 5.2$ cylinders with strong fourfold correlations (centre), and nematic state formed by $\mathcal{A} = 10.4$ rolling pins.

of the orientational ordering due to the limited statistics that are forced upon us by the large size of the rice grains.

Figure 5 shows the region of phase space explored and gives us an overview of the results. The cylinders, irrespective of aspect ratio, displayed strong fourfold orientational, i.e., tetratic, correlations. Studies of the area-fraction dependence of these correlations, presented in section 3.1, were done using the shorter rods: since the system size measured in terms of particle length was greater for the short particles, they were less sensitive to the nature of the boundary and offered better statistics. We observed short-ranged tetratic order, but with large correlation lengths. The high-aspect-ratio rolling pins formed nematic phases with quasi-long-range order with power-law decay of orientational correlations.
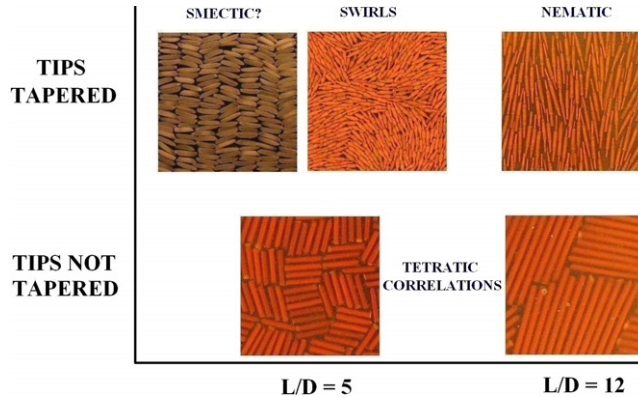
Figure 5. Schematic overview of parameter space explored and steady states in each region. The vertical axis represents the two different shapes of the particles we used.

The low-aspect-ratio rolling pins formed swirly states, which we discuss in section 3.4.2. Common to both nematic and tetratic states was the tendency to rotate globally and persistently in one direction, presumably in response to some asymmetry in the boundaries of the system. This distinguishes this phenomenon from that observed by [24] who also observe globally rotating phases, only the particles forming their phase are, unlike ours, intrinsically chiral. We discuss this in section 3.4.1. We also observed striped, smectic-like phases in experiments using rice grains. Interestingly, we have not been able to observe the stripes using bails or cylinders with the same aspect ratio as the rice.

3.1. Towards the tetratic phase

Over the range of concentration and other parameters explored, the strictly cylindrical particles (i.e., flat headed, neither tapered like the 'bails' that showed nematic order, nor spherically capped like the spherocylinders widely studied in simulations) did not form ordered phases. However, their isotropic phase showed tetratic, that is, fourfold orientational, short-range order unaccompanied by nematic correlations. The range of tetratic correlations increased substantially with increasing area fraction. The correlation function evaluated was $G_4(r) = \langle \cos[4(\theta_i - \theta_j)] \rangle$, where θ_i is the orientation of the rods with respect to some arbitrary, pre-selected axis. i and j are particle indices that run from 1 to the number of particles, N. The angular brackets are a time average, over pairs i, j of particles separated by a distance r. For each pair, we calculate G_4 as a function of $r_\perp$ and $r_\parallel$, which are, respectively, the components of the separation vector **r** between the rod centres perpendicular and parallel to the cylinders' long axes. $r_\perp$ and $r_\parallel$ are distinct for each particle in a given pair; they have to be evaluated for each particle, rather than each particle pair, as would have been sufficient if G_4 were evaluated as a function of the scalar distance, r.

Both long ($\mathcal{A} = 12.6$) and short ($\mathcal{A} = 5.2$) cylinders showed tetratic correlations as shown in figure 6. The range of tetratic order is shorter (when distance is scaled by cylinder length) for the long cylinders; however, even a correlation length $\xi = 1.57L = 19.8D$, as found for the long cylinders, indicates substantial tetratic ordering with clearly identifiable
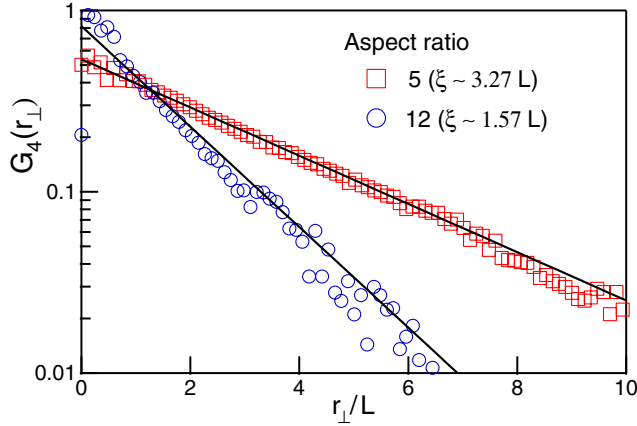
Figure 6. Tetratic correlation lengths (scaled by rod length L) are larger for aspect ratio $\mathcal{A} = 5.2$ than for $\mathcal{A} = 12.6$. Results shown for area fractions 87% and correlations as functions of $r_\perp$ (defined in section 3.1); the behaviour with respect to $r_\parallel$ is similar.
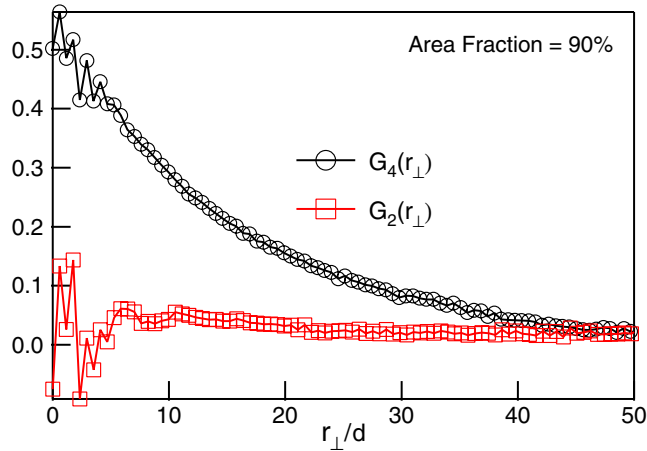

Figure 7. Substantial $G_4(r)$ and very small $G_2(r)$ for cylinders ($\mathcal{A} = 5.2$) at area fraction 90% confirm that the correlations are tetratic, not angular harmonics in twofold ordered states.

fourfold motifs as seen in figure 5. When the experiments were performed in a square, rather than a circular frame, one might have expected fourfold orientational order to be in general enhanced, since alignment parallel to the walls is (see section 1) favoured by the mechanics of collisions with the wall. We find that this is true for both long and short cylinders but not at all for the bails.

To distinguish between tetratic and nematic ordering, we have plotted for the short cylinders $\mathcal{A} = 5.2$ at area fraction 90% $G_4(r)$ and $G_2(r)$ in figure 7; here $G_2(r) = \langle\cos[2(\theta_i - \theta_j)]\rangle$ quantifies the extent of nematic ordering. $G_4(r)$ clearly dominates, and nematic correlations are negligible. This confirms what is apparent from the real space image of the tetratic phase, figure 4. We are thus seeing true fourfold correlations, not angular harmonics of twofold correlations.
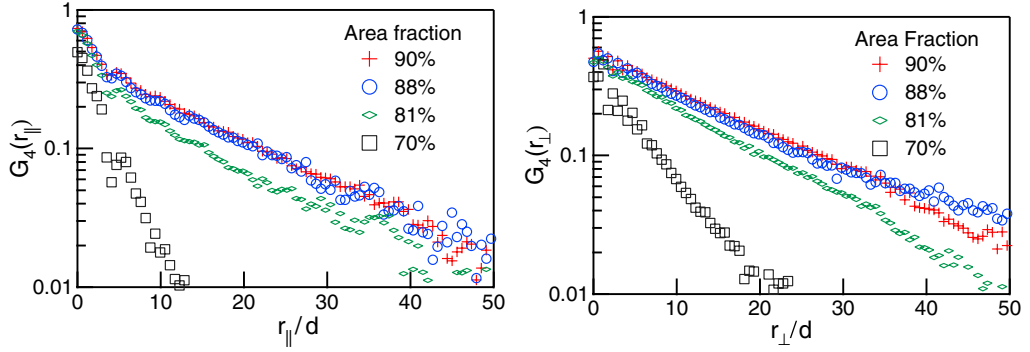
Figure 8. G_4 (defined in section 3.1) as a function of $r_\perp$ and $r_\parallel$ for different area fractions, for cylinders with aspect ratio 5.
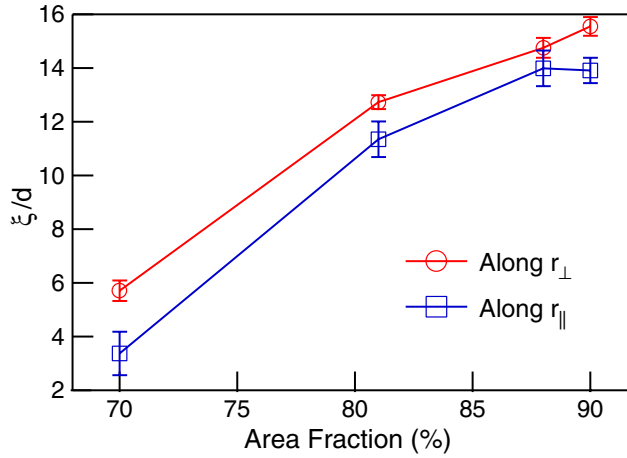

Figure 9. Tetratic correlation lengths increase with area fraction, suggesting that a tetratic phase should appear if some other parameter such as shaking amplitude is varied. We do not know the origin of the slight difference between the correlation lengths obtained along $r_\perp$ and $r_\parallel$.

We now present the dependence of the range of tetratic correlations on area fraction for the short cylinders ($\mathcal{A} = 5.2$). Figure 8 shows G_4 as a function of $r_\parallel$ and $r_\perp$ for various area fractions. The range of tetratic correlations increases monotonically with area fraction, as shown in figure 9, which displays the correlation length, ξ, extracted from figure 8. The ξ obtained from $r_\perp$ and $r_\parallel$ show the same qualitative behaviour, but are slightly different in magnitude.

The correlation lengths are substantial at high area fractions, indicating a high tetratic susceptibility, and the likelihood that a quasi-long-ranged tetratic phase lurks nearby in parameter space. However, it remains to be determined which parameter—area fraction, confinement thickness, vibration amplitude or frequency—will most easily take the system across this conjectured isotropic–tetratic phase boundary. We reiterate that the tetratic ordering is a strong function of particle shape; by way of comparison, the equilibrium phase diagram of [1] for discorectangles at similar aspect ratios shows no tendency to tetratic order. They find isotropic, nematic, and crystalline phases, none of which we

Table 2. The table below lists the correlation lengths ξ (scaled by D, the rod thickness) and decay exponents α for, respectively, the short-range-ordered and power-law-ordered nematic phases.

Area fraction	$\xi(r_\parallel)/D$	$\xi(r_\perp)/D$	$\alpha(r_\parallel)$	$\alpha(r_\perp)$
50%	69	64	—	—
60%	—	—	$0.0113 \pm 4\mathrm{e}{-4}$	$0.0182 \pm 8\mathrm{e}{-4}$
70%	—	—	$0.0066 \pm 3\mathrm{e}{-4}$	$0.0140 \pm 5\mathrm{e}{-4}$

see with rectangles. This difference could be a nonequilibrium effect rather than a shape effect; however, as we will see in section 3.2, tapered particles order differently. Also, Monte Carlo simulations of rectangles [21] at much smaller aspect ratio, $\mathcal{A} = 2$, reveal a true tetratic phase. While it is not clear at all whether this equilibrium phase will survive to the large $\mathcal{A}$ regime, we hope that our results will stimulate equilibrium simulations of this region of parameter space.

3.2. The nematic phase

Why do cylinders not show nematic order even when they are extremely long? Nematic order is typically investigated in simulations using spherocylinders, discorectangles, or ellipsoids, all of which have narrower tips than waists and can thus interdigitate, promoting uniaxial alignment. This indicates that the rod tips needed to be tapered to obtain a nematic phase. We therefore used the particles labelled 'bails' in figure 1, with aspect ratio $\mathcal{A} = 10.4$, since equilibrium Monte Carlo studies tell us that $\mathcal{A} > 7$ is needed to produce a two-dimensional nematic.

As is evident from the real space images (figure 4) the long bails do indeed show nematic correlations. The tendency to nematic order is quantified in figure 10, which shows G_2 as a function of $r_\perp$ and $r_\parallel$ for three different area fractions ϕ. Here $G_2(r) = \langle\cos[2(\theta_i - \theta_j)]\rangle$. The symbols are the same as defined in section 3.1. The system shows a high degree of order at each of these area fractions. The decay of G_2 was consistent with a power law for all three values of ϕ, although the decay exponents (listed in table 2) were exceedingly small for the two higher values of ϕ.

Given the small system sizes in our experiment, we expect strong finite-size effects. In order to assess more precisely whether the correlations were long ranged, power law, or short ranged with very long correlation lengths, we performed a subsystem analysis of the cumulants following [26]. The quantities evaluated were $S = \langle\psi\rangle_L$, where ψ is the order parameter ($\psi = \frac{1}{N_L}\sum \mathrm{e}^{i2\theta_j}$, where j runs over the number N_L of particles within the subsystem defined by L) and L is the linear size of the subsystem over which S was evaluated, $S^2 = \langle\psi^2\rangle_L$ and $S^4 = \langle\psi^4\rangle_L$. The Binder reduced cumulant, $U_L = 1 - \frac{\langle S^4\rangle}{3\langle S^2\rangle^2}$ was then evaluated. The results are plotted as a function of area fraction, ϕ, for different subsystem sizes L in figure 11.

As shown in [26], for phases with LRO the curves for different system sizes L will cross at a certain value of area fraction $\phi = \phi^*$. If there is QLRO, the curves of U_L versus ϕ for different L should collapse onto a single line over an extended range of values of ϕ. The lower limit of this value will be ϕ^*, the isotropic–nematic transition value.
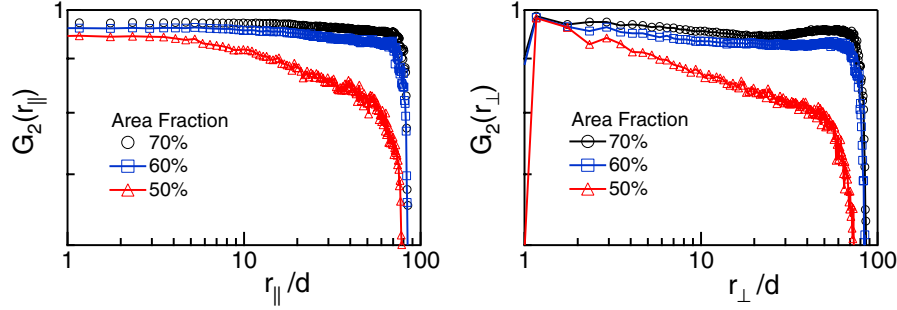
Figure 10. $G_2(r)$ (defined in section 3.2) as a function of $r_\parallel$ and $r_\perp$: The phases are very highly ordered and only a detailed subsystem analysis confirmed the quasi-long-ranged (rather than true-long-ranged) order at area fraction $\phi = 60\%$ and 70% and short-ranged correlations at $\phi = 50\%$. The decay exponents and correlation lengths extracted from the plots are summarized in table 2.
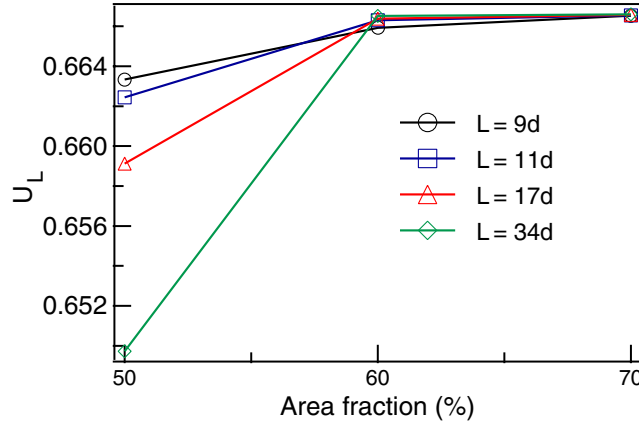

Figure 11. Binder reduced cumulant U_L versus area fraction suggests quasi-long-range nematic order at and above $\phi = 60\%$, short-ranged order below. Here L is the linear size of the subsystem in units of the rod diameter d.

Figure 11 suggests that the phases formed at the higher area fractions do show QLRO and the isotropic–nematic transition occurs at an area fraction somewhere between 50% and 60%. In figure 12 we show the Binder cumulant as a function of subsystem sizes L, for different area fractions, ϕ. The downturn at large L for $\phi = 50\%$ indicates short-range order. We show a greatly magnified version of this plot for the two higher area fractions as an inset. U_L for 70% is slightly but systematically larger than that for 60%. This difference is at the edge of our resolution, but it leaves open the tempting possibility that these nonequilibrium nematics have true, rather than quasi-long-range order. Further measurements on large systems are required to settle this important question of principle.

3.2.1. Varying amplitude of oscillation. The presence of a third dimension into which the particle is lofted means that the two-dimensional projections of the particles can overlap, and that unlike hard particles a temperature variable could be relevant to the order. As we said in section 2.2, the shaking amplitude a_0 could act as a kind of temperature. A natural
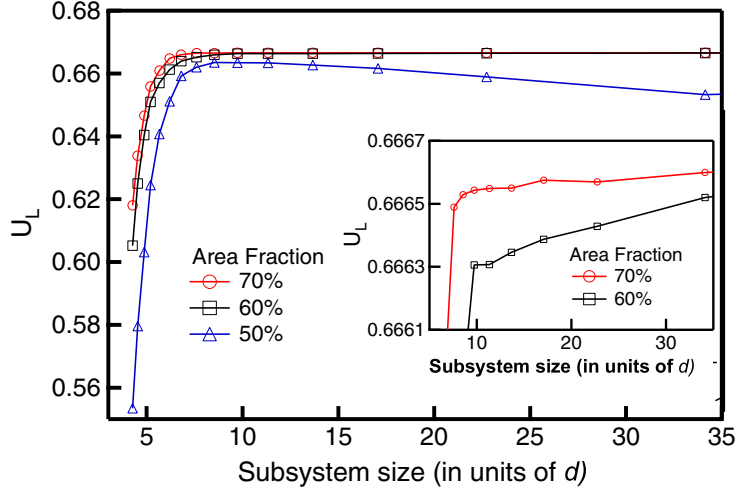
Figure 12. Binder reduced cumulant U_L versus linear size L of subsystem over which U_L was evaluated. For $\phi = 50\%$, mild dip in curve suggests short-ranged order. Inset: U_L for $\phi = 60\%$ and 70% at a higher resolution. ϕ is very slightly, but systematically higher for $\phi = 70\%$, leaving open the possibility of true long-range nematic order in this driven two-dimensional systems. Here L is the linear size of the subsystem in units of the rod diameter d.
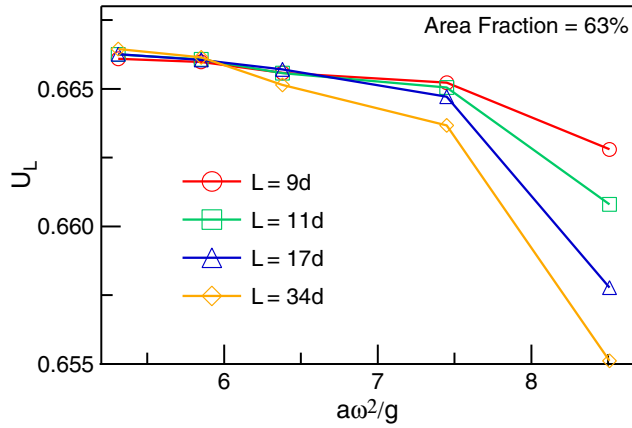

Figure 13. Binder reduced cumulant U_L versus dimensionless acceleration. The loss of long-ranged order upon increasing amplitude confirms the notion that a temperature variable is relevant in this system and is related to the shaking strength.

dimensionless measure of how strongly the system is being shaken is $\Gamma \equiv (2\pi f)^2 a_0/g$, where f and g are, respectively, the oscillation frequency and the acceleration due to gravity. We studied the effect on the nematic order of changing acceleration while holding fixed the gap height, H, and particle diameter, D; changing these would have changed the inter-penetrability of the particles in two dimensions.

Figure 13 shows the Binder reduced cumulant of the phase as a function of dimensionless acceleration. The area fraction of the phase is about 63%, within the

nematic regime identified in figure 12. The acceleration is varied by holding the frequency, f, fixed and varying the amplitude, a_0. Even though $a_0 \ll (H - D)$ over the entire range of amplitudes, the higher shaking amplitudes do affect the extent of order in the system. This is not entirely surprising: while a_0 is small, the ratio of the characteristic kinetic energy $1/2m(2\pi f a_0)^2$ and the maximum possible potential energy $mg(H - D)$ varies from 0.2 to 0.36 over the range of the plot. However, as can be seen by the small range of vertical axis, the degree to which the phase disorders by increasing Γ from 5 to 8 is much less than that achieved by reducing the area fraction from 70% to 50%.

3.3. Two-dimensional smectic order?

Our observations on basmati rice gave images with strong indications of striped, i.e., smectic order (see figure 4). In two-dimensional systems at thermal equilibrium, we know that thermal fluctuations render smectic order strictly short ranged, while in three-dimensional systems it is quasi-long-ranged. These conclusions are based on derivations of the variance of layer displacement fluctuations from an elastic free-energy functional, in which, as a consequence of rotation invariance, the cost of layer displacements with wavevector $\mathbf{q}$ parallel to the layers varies as q^4. Since the systems we are studying are driven, not thermal equilibrium, these arguments do not apply *a priori*, and the possibility of quasi-long-range (or, for that matter, true long-range) smectic order in our vibrated granular-rod monolayers remains open. We are studying this possibility theoretically [27]. Experimentally, however, our systems are not large enough for the type of analysis (see, e.g., [28, 29]) required to check whether the images we are seeing are true smectics, weakly ordered two-dimensional crystals, or smectics disordered by the presence a finite but small density of free dislocations (which would be nematics on large length scales).

3.4. Dynamical nonequilibrium phenomena

3.4.1. Collective, coherent rotation. All the phases showed a marked tendency to rotate globally. For the nematic phases, the square frame prevented them from rotating (except in certain cases, which we shall come to in the next paragraph), but we could not prevent the tetratic phase from rotating, in part because we did not use a square frame, since we wanted to see how strong the tetratic correlations were in the absence of such externally imposed fourfold alignment.

Since this is a nonequilibrium system, any stray chirality in the system, even at the boundary, should result [30] in macroscopic circulation. The observed global rotation is thus a signature of the driven nature of the system. A thermal equilibrium system, no matter how chirally asymmetric, would not display persistent currents. Our observed rotation rates were of the order of a degree in 10^4 cycles of oscillation. In one instance, when we were using the bails in the square boundary (where, under normal circumstances, the rotations are curbed), the phase began rotating fast, turning through a degree in $\approx 10^3$ cycles of oscillation. The source of the asymmetry appeared to be a slight misalignment of the particles fixed at the boundary, because we were able to stop the rotation by aligning them more carefully. That this minor imperfection in boundary alignment could have such a strong effect was a surprise, and means the rotation phenomenon merits more serious investigation.

3.4.2. Swirls. Since *basmati* rice (aspect ratio $\mathcal{A} = 4.2$) showed smectic tendencies, we studied tapered copper rods with similar aspect ratio (aspect ratio $\mathcal{A} = 4.9$) but half the length of the rice grains, in the hope of getting a larger number of smectic layers in the sample cell. Unexpectedly, we found no sign of smectic layering. Instead, a very dynamic pattern of swirls appeared, reminiscent of bacterial swimming patterns [31]. The swirly state looks like a defect-ridden nematic, which is curious because equilibrium Monte Carlo studies on rods in two dimensions suggest that nematics should not form for aspect ratios less than seven. These swirls, which are strength $\pm 1/2$ disclinations, differ from those seen in [15]: the latter are of unit strength, they have a core that looks like a crystalline packing of standing rods, and each defect is chiral because the rods have a systematic tilt in the direction of their tangential velocity in the region outside the core. In our case, the circulation appears to be a result of the interaction between defects. It remains to be seen whether we are seeing coarsening towards a nematic, the disordering of a nematic (i.e., coarsening towards the isotropic phase), or simply a disordered, correlated, defect-turbulent steady state.

4. Conclusion and discussion

This paper has presented an exploration of the collective properties of vibrated rods in two dimensions, focusing on orientationally ordered phases. Tapered particles lead to nematic order at large area fractions, in keeping with the thermal equilibrium Monte Carlo studies of [1], while strictly cylindrical particles, with flat tips, display strong tetratic correlations over a very broad range of aspect ratios. It remains to be established whether the strong sensitivity to particle shape is a nonequilibrium phenomenon or whether it can be reproduced in equilibrium simulations. We also observed some clearly nonequilibrium phenomena: persistent, systematic rotation of the entire phase, presumably as a result of stray chirality in the system, and also a rich pattern of circulating disclinations of strength $\pm 1/2$. Detailed quantitative analyses of the dynamics of the swirls, of tagged-particle motion and time-dependent correlations of collective modes and other nonequilibrium effects will appear in a separate paper [27].

References

[1] Bates M A and Frenkel D, 2000 *J. Chem. Phys.* **112** 10034
[2] Vicsek T, 1995 *Phys. Rev. Lett.* **75** 1226
   Czirok A, Stanley H E and Vicsek T, 1990 *J. Phys. A: Math. Gen.* **30** 1375
   Vicsek T, Czirok A, Ben-Jacob E, Cohen I and Shochet O, 1995 *Phys. Rev. Lett.* **75** 1226
[3] Toner J and Tu Y, 1995 *Phys. Rev. Lett.* **75** 4326
   Tu Y, Ulm M and Toner J, 1998 *Phys. Rev. Lett.* **80** 4819
   Toner J and Tu Y, 1998 *Phys. Rev.* E **58** 4828
[4] Ramaswamy S, Simha R A and Toner J, 2003 *Europhys. Lett.* **62** 196
[5] Lee H Y and Kardar M, 2001 *Phys. Rev.* E **64** 056113
[6] Liverpool B and Marchetti M C, 2003 *Phys. Rev. Lett.* **90** 138102 (http://arxiv.org/abs/cond-mat/0406276)
[7] Sankararaman S, Menon G I and Sunil Kumar P B, 2004 *Phys. Rev.* E **70** 031905
[8] Aranson I S and Tsimring L S, 2005 *Phys. Rev.* E **71** 050901
[9] Toner J, Tu Y and Ramaswamy S, 2005 *Ann. Phys.* **318** 170
[10] Aranson I S and Tsimring L S, 2005 http://arxiv.org/abs/cond-mat/0507419
[11] Mounfield C C and Edwards S F, 1994 *Physica* A **210** 279
[12] Buchalter B K and Mark Bradley R, 1992 *Phys. Rev.* A **46** 3046
[13] Stokely K, Diacou A and Franklin S V, 2003 *Phys. Rev.* E **67** 051302
[14] Villarruel F X, Lauderdale B E, Mueth D M and Jaeger H M, 2000 *Phys. Rev.* E **61** 6914
[15] Blair D L, Neicu T and Kudrolli A, 2003 *Phys. Rev.* E **67** 031303
[16] Aranson I S and Tsimring L S, 2003 *Phys. Rev.* E **67** 021305
[17] Galanis J, Harries D, Sackett D L, Losert W and Nossal R, 2005 http://arxiv.org/abs/cond-mat/0508202
[18] Fraden S, 2005 private communication
[19] Lagomarsino M C, Dogterom M and Dijkstra M, 2003 *J. Chem. Phys.* **119** 3535
[20] Khandkar M and Barma M, 2005 *Phys. Rev.* E at press (http://arxiv.org/abs/cond-mat/0502200)
[21] Donev A, Burton J, Stillinger F H and Torquato S, http://arxiv.org/abs/cond-mat/0508550
[22] Veerman J A C and Frenkel D, 1992 *Phys. Rev.* A **45** 5632
[23] Borukhov I, Bruinsma R F, Gelbart W M and Liu A J, 2005 *Proc. Nat. Acad. Sci.* **102** 3673
[24] Tsai J-C, Ye Fangfu, Rodriguez J, Gollub J P and Lubensky T C, 2005 *Phys. Rev. Lett.* **94** 214301
[25] http://rsb.info.nih.gov/ij/
[26] Weber H, Marx D and Binder K, 1995 *Phys. Rev.* B **51** 14636
[27] Narayan V, Menon N and Ramaswamy S, 2005 unpublished
[28] Caillé A, 1972 *C. R. Acad. Sci.* B **274** 891
[29] Safinya C R, Roux D, Smith G S, Sinha S K, Dimon P, Clark N A and Bellocq A M, 1986 *Phys. Rev. Lett.* **57** 2718
[30] Curie P, 1894 *J. Physique* III **3** 393
[31] Dombrowski C, Cisneros L, Chatkaew S, Goldstein R and Kessler J O, 2004 *Phys. Rev. Lett.* **93** 098103